

Article

Microstructure and High-Temperature Properties of TC31 Alloy Manufactured by Laser Melting Deposition

Hepeng Li ^{1,2,*}, Bin Guo ¹, Yingying Zong ¹ and Debin Shan ¹

¹ School of Materials Science and Engineering, Harbin Institute of Technology, Harbin 150001, China; bguo@hit.edu.cn (B.G.); hagongda@hit.edu.cn (Y.Z.); shandb@hit.edu.cn (D.S.)

² Beijing Xinghang Electro-Mechanical Equipment Co., Ltd., Beijing 100074, China

* Correspondence: lhp_159@126.com; Tel.: +86-10-68741413

Abstract: This paper presents a comprehensive study conducted to optimize the mechanical properties for a laser-melting-deposition fabricated TC31 (Ti-Al-Sn-Zr-Mo-Nb-W-Si) alloy, which is a newly developed high-temperature alloy used in the aerospace industry. The results showed that the laser melting deposition (LMD)-built sample exhibited columnar structures with very fine α -laths inside. Annealing and solution treatment resulted in an $\alpha+\beta$ lamellar structure consisting of α -laths and β -films, of which thicknesses depended on the temperature. Solution treatment and subsequent aging did not significantly change the lamellar structure. However, aging at 650 °C led to the formation of nanoscale α precipitates within the remaining β , while aging at 750 °C resulted in coarse α precipitates. The solution-treated samples exhibited the best combination of strength and ductility at room temperature, ultimate tensile strength of 1047 MPa, and elongation of 13.0%, which is superior to the wrought TC31 counterparts. The sample after solution treatment at 980 °C and subsequent aging at 650 °C obtained an attractive combination of strength and ductility both at room temperature and high temperature due to the synergistic effect of the soft $\alpha + \beta$ lamellar structure and hard fine α precipitates. These findings provide valuable information on developments of LMD-built TC31 alloy for aerospace applications and shed light on AM of other titanium alloys with desirable high-temperature properties.

Keywords: laser melting deposition; TC31 alloy; alpha phase; post-heat treatments; high-temperature properties; microstructure–tensile properties relationship



Citation: Li, H.; Guo, B.; Zong, Y.; Shan, D. Microstructure and High-Temperature Properties of TC31 Alloy Manufactured by Laser Melting Deposition. *Crystals* **2022**, *12*, 475. <https://doi.org/10.3390/cryst12040475>

Academic Editor: Anna Paola Caricato

Received: 20 February 2022

Accepted: 22 March 2022

Published: 30 March 2022

Publisher's Note: MDPI stays neutral with regard to jurisdictional claims in published maps and institutional affiliations.



Copyright: © 2022 by the authors. Licensee MDPI, Basel, Switzerland. This article is an open access article distributed under the terms and conditions of the Creative Commons Attribution (CC BY) license (<https://creativecommons.org/licenses/by/4.0/>).

1. Introduction

Titanium alloys are extensively used as key structural components in the aerospace industries because of their specific combination of strength, lightweight, and resistance to aggressive environments [1,2]. These components are usually fabricated by conventional processes at a very high buy-to-fly ratio and low material utilization ratio [3]. Recently, the emerging technique, additive manufacturing (AM), is highly effective in reducing production time and cost compared to traditional methods, which also get great attention towards manufacturing of highly complex structural geometries and significant strengthening [4–10].

LMD is an advanced AM technique that allows direct fabrication of full density near-net-shape metal components based on coaxial powder-delivery layer-on-layer deposition [11]. This process is characterized by a large temperature gradient and rapid cooling rate, which, thus, result in large columnar prior β grains and fine basket-weave microstructure [12]. This microstructure normally exhibits high strength and low ductility, and significant mechanical anisotropy [13–16]. Many studies have been conducted to investigate microstructures and mechanical properties of LMD titanium alloys, mostly on Ti-6Al-4V [16–18] and Ti-6.5Al-3.5Mo-1.5Zr-0.3Si alloy [15,19]. For example, Carroll et al. [16] investigated the anisotropic mechanical properties of Ti-6Al-4V fabricated by

LMD. Ren et al. [20] investigated the microstructure and tensile deformation behavior of Ti-6Al-4V alloy fabricated using a high-power LMD. They reported that the post-heat-treated microstructure consisted of coarse columnar prior- β grains and α -laths, which caused large elongation (~18%) superior to the conventional Ti-6Al-4V alloy. Wolff et al. [21] investigated the relationships between the process parameters and the resulting mechanical behavior of LMD-processed Ti-6Al-4V. Keist et al. [14] studied the role of geometry on properties of Ti-6Al-4V structures fabricated using LMD. Zhao et al. [22] studied the effect of post-heat treatment on the microstructure and tensile properties of LMD-processed Ti-6Al-4V. They reported that a largely improved ductility (25% total elongation) with a comparable tensile strength (860 MPa) was obtained using a triple heat treatment. The previous studies suggest that LMD-fabricated Ti-6Al-4V alloy exhibited superior mechanical properties comparable to that of conventionally processed counterparts [23,24]. Post treatments such as hot isotactic pressing and heat treatments can improve the ductility by changing the microstructure [24,25].

TC31 (Ti-Al-Sn-Zr-Mo-Nb-W-Si) is a new $\alpha + \beta$ high-temperature titanium alloy, which exhibits high specific strength and creep resistance at temperatures from 600 to 700 °C. It has become one of the competitive candidates for the skin and air inlet components of hypersonic aircraft [26–28]. It has been reported that the ultimate tensile strength (UTS) of this alloy at 650 °C was approximately 600 MPa, which is almost equal to the UTS of Ti-1100 and BT36 at 600 °C (630 MPa for Ti-1100 and 640 MPa for BT36) [26,29]. However, to the best of the authors' knowledge, the microstructure and mechanical properties of TC31 fabricated by AM have never been studied. TC31 alloy fabricated using AM methods may exhibit different microstructures and mechanical properties from that of Ti-6Al-4V alloy because of the large differences in chemical composition.

Therefore, TC31 bulk samples were fabricated by the LMD process in this study. Microstructural features of the LMD TC31 samples before and after post-heat treatments were investigated by using an optical microscope (OM), scanning electron microscope (SEM), and electron backscatter diffraction (EBSD). Mechanical properties at room temperature and high temperature of 600 and 650 °C of the heat-treated samples were evaluated. The effect of post-heat treatments on the microstructure and mechanical properties of LMD TC31 samples was investigated. The room-temperature and high-temperature tensile properties were also compared with the conventional wrought counterparts.

2. Materials and Experimental

The feedstock used to fabricate the samples was a pre-alloyed TC31 powder produced by a plasma rotating electrode process from Avimetal Powder Metallurgy Technology Co. Ltd. (Beijing, China). The powders had a spherical shape and a size ranging from 75 to 180 μm , as shown in Figure 1a. The chemical compositions of the powders are shown in Table 1.

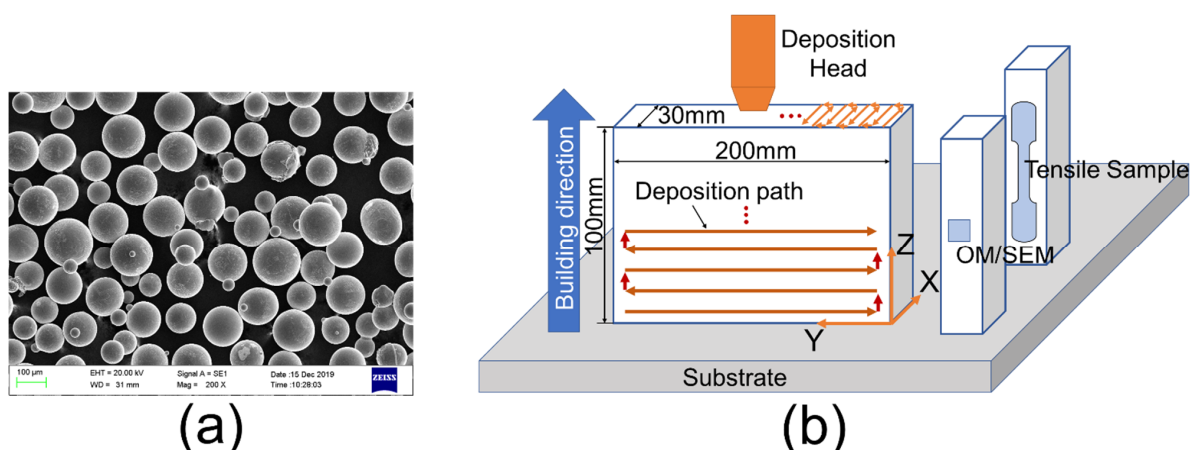


Figure 1. (a) The SEM of the TC 31 alloy powder and (b) the sample orientation and deposition strategy.

Table 1. Chemical composition (wt.%) of the alloy powders.

Al	Sn	Zr	Mo	Nb	W	Si	Fe	C	N	H	O	Ti
6.79	2.9	3.1	1.09	1.11	0.46	0.13	0.046	0.008	0.011	0.0014	0.14	Bal.

Samples with a dimension of $200 \times 30 \times 100$ mm were manufactured using an LMD machine (LMD-8060). The samples were fabricated with the following parameters: 300 W of laser power, 0.85 m/min of scan speed, 250 μm of layer thickness, 500 μm of spacing, and 1.5 g/min of powder distribution rate. Scan strategy and sample orientation are shown in Figure 1b. During deposition, high purity argon gas was used for the powder flow (2 L/min), coaxial gas (9 L/min), and shielding gas (5 L/min). O content in the chamber was controlled below 5×10^{-5} during the process. All samples were deposited on a TC31 substrate plate. The as-build samples were stress relieved via a heat treatment at 650 °C for 3 h followed by furnace cooling.

The β -transus temperature was measured to be 1010–1020 °C through a metallography method. Post-heat treatments of the samples were conducted in a preheated tube furnace. Simple annealing was conducted at 800 °C for 2 h and followed by air cooling. Solution treatment was performed at 980 °C and held for 2 h, followed by air cooling. This sample is referred to as the ST sample. The samples after solution treatment at 980 °C were also subjected to aging at 650 and 750 °C for 2 h, followed by air cooling. They are referred to as the STA1 and STA2 samples, respectively.

The samples for microstructural observation were mechanically ground and polished. The finished samples were etched in a Kroll etchant for optical metallographic (OM) observation using an OLYMPUS BX51. Microstructural observations were also performed using electron back-scattered diffraction (EBSD) mapping and backscatter electron (BSE) imaging. EBSD maps were taken using a field emission scanning electron microscope (FE-SEM: JSM-7100F) operated at 20 kV at a working distance of 15 mm and a step size of 0.2 μm . BSE imaging was performed using an FE-SEM (TESCAN MIRA III) operated at 20 kV with a working distance of 10 mm.

The samples for both room-temperature and high-temperature tensile testing had a gauge dimension of $\phi 5 \times 25$ mm and were machined along the build direction, as shown in Figure 1b. The room-temperature tensile tests were carried out using an MTS E45 tensile machine at a constant strain rate of 1×10^{-3} , which was determined by a contact extensometer. The high-temperature (at 600 and 650 °C) tensile tests were performed using the same machine at strain rates of 1×10^{-4} and 2×10^{-3} before and after yielding, respectively. During the high-temperature tensile test, the heating rate was 50 °C/min and the soaking time before the test was 5 min. The tensile tests were repeated three times for each condition and the average values of the ultimate tensile strength (UTS), yield strength (YS), and elongation (El) were reported.

3. Results and Discussion

3.1. Microstructures

Three-dimensional meso- and microstructures of the as-build samples are shown in Figure 2. The mesostructure is primarily dominated by columnar β grains. As shown in Figure 2a, the prior β grains are either aligned or slightly inclined to the building direction, on the YZ and XZ planes, while they exhibit an equiaxed grain shape on the XY plane. They tended to epitaxially grow along the building direction, owing to the high-temperature gradient during laser deposition [11]. The columnar grains exhibit a thickness of approximately 100–200 μm on both of the YZ and XZ planes. High-magnification OM images in Figure 2b reveal that the microstructure within the columnar grains is dominated by fine lamellar α grains having a thickness of approximately 1 μm . This kind of structure is typically observed in additively manufactured $\alpha + \beta$ titanium alloys [16,22].

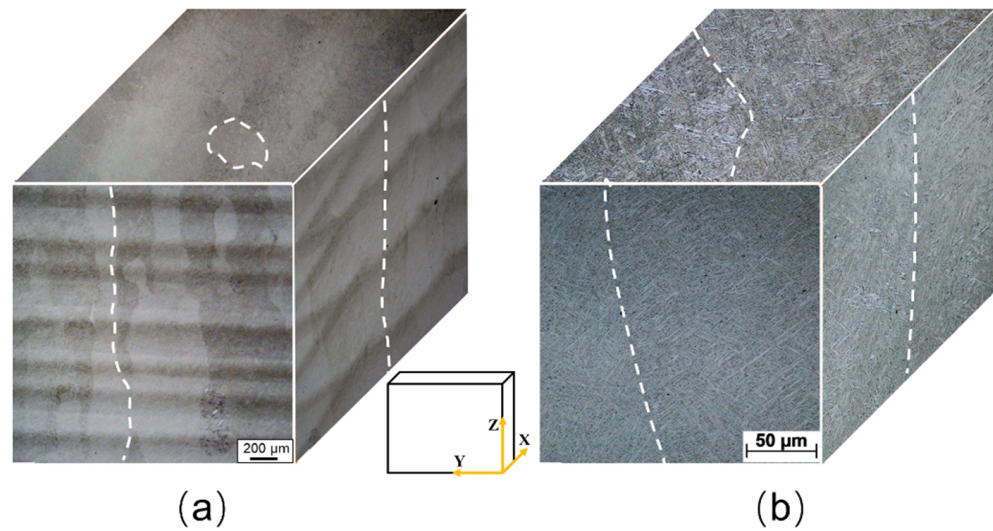


Figure 2. Three-dimensional optical microscopy view of the as-built sample, (a) low- and (b) high-magnification, which was dominated by columnar β grains.

Figure 3 shows the microstructures of the annealed and solution-treated samples. When annealed at 800 °C, the martensites were completely decomposed into α and β . Grain boundary α (α_{gb}) was formed in the shape of continuous layers at the original columnar boundaries, as shown in Figure 3a. The annealed sample exhibited a fine $\alpha + \beta$ lamellar structure consisting of thin α -laths and β -films, as shown in Figure 3b. The thickness of α -laths was revealed at the scale of approximately 1 μm . EBSD maps in Figure 3c also confirmed the fine-scale of the lamellar structure. In addition, the original β grains contained three to four different variants. When solution treated at 980 °C, the sample exhibited a higher fraction of β phase, as shown in Figure 3d. α_{gb} layers were also formed in this sample, however, some of them exhibited an equiaxed shape. Thickening and shortening occurred in terms of the α -laths, exhibiting a thickness of 2–3 μm , as shown in Figure 3e. In addition to the α -laths, some equiaxed α grains with a size of approximately 5 μm were formed at this temperature, as shown in Figure 3e,f.

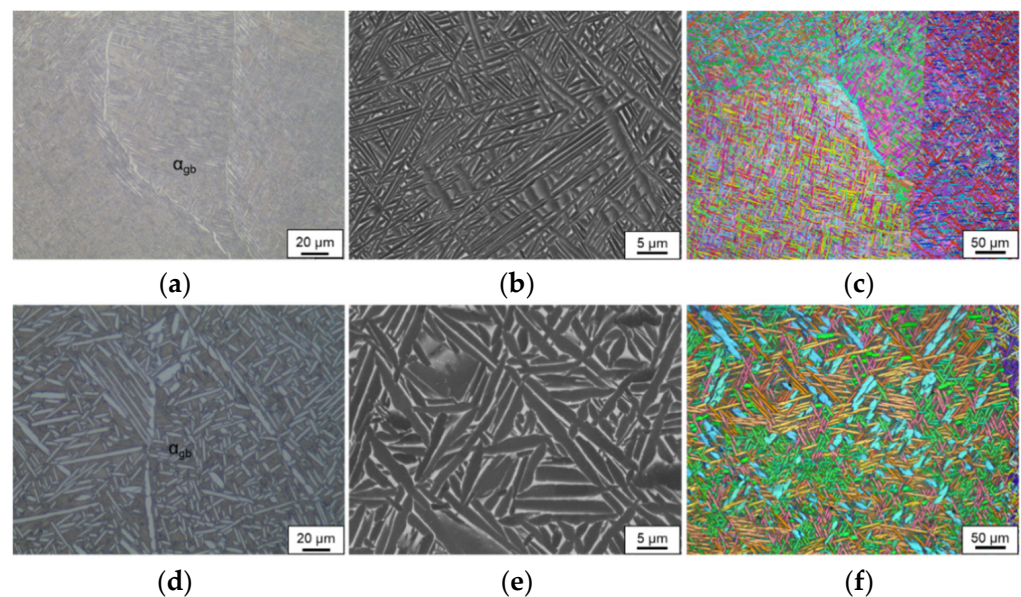


Figure 3. The alpha phase microstructures of the samples annealed at 800 °C (a–c) and solution treated at 980 °C (d–f).

Figure 4 shows the microstructures of the solution-treated and aged samples. The samples after aging at 650 and 750 °C exhibited similar microstructures to that of the solution-treated sample, as seen from OM images in Figure 4a,d. The aging treatment at 650 and 750 °C did not significantly change the morphology of the primary α laths, as shown in Figure 4b,e. However, very fine-scaled secondary α (α_s) was precipitated within the β regions in an acicular shape, as shown in Figure 4c,f. In addition, the α_s in the sample aged at 750 °C exhibited a coarser size compared to that in the sample aged at 650 °C.

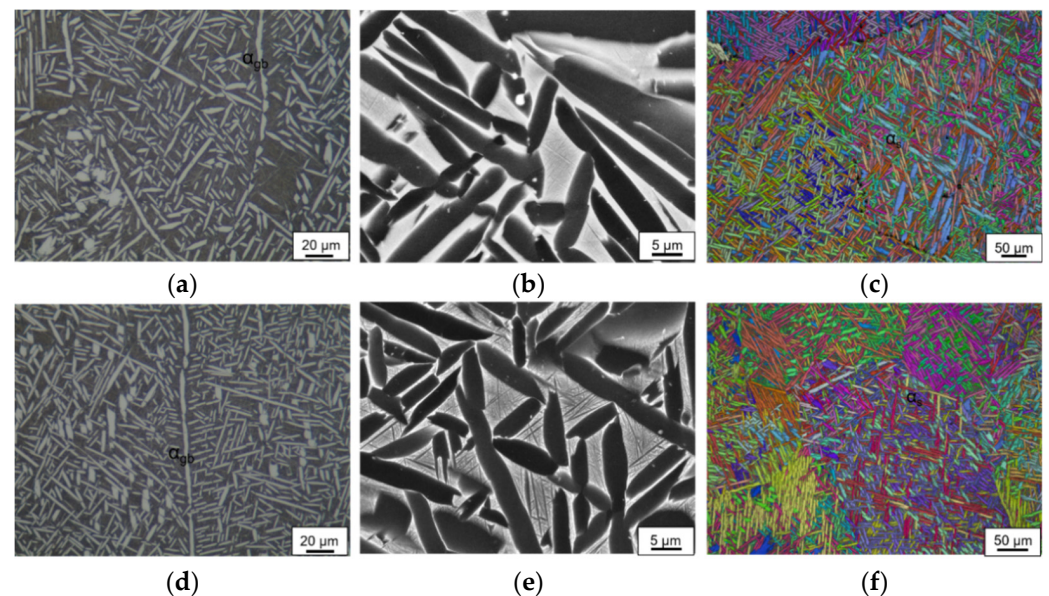


Figure 4. Alpha phases morphology in the samples after solution treatment at 980 °C and aged at 650 (a–c) and 750 °C (d–f).

3.2. Tensile Properties

Tensile properties of the samples tested at room temperature and high temperatures of 600 and 650 °C are shown in Figure 5. At room temperature, the samples after post-heat treatments exhibited a similar strength level, i.e., UTS of 1050–1100 MPa and YS of approximately 1000 MPa. However, the ductility strongly depended on the heat treatment. The ST exhibited the highest El of 13% and the annealed sample exhibited the lowest El of less than 5%. The STA1 sample exhibited slightly higher strength than that of the ST sample, accompanied by a large loss of room-temperature ductility. The STA2 sample exhibited similar strength and ductility to that of the ST sample because the aging at 750 °C resulted in coarse secondary α precipitates in the remaining β regions, as shown in Figure 4e.

At 600 °C, the annealed and ST samples showed similar strength and ductility, for example, UTS of 700 MP, YS of 600 MPa, and El of 27.5%, as shown in Figure 5b. After aging, the strength and ductility of the samples depended on the aging temperature. For example, the STA1 sample aged at 650 °C resulted in a slight increase in YS; however, aging at 750 °C resulted in a decrease in YS. This is similar to the case at room temperature. Except for the STA2 sample, the other samples at 600 °C exhibited UTS values higher than 650 MPa and ductility values higher than 25%.

At 650 °C, the annealed, ST, and STA1 samples exhibited similar strength levels of approximately 630 MPa in UTS and 450 MPa in YS, but they showed significantly different ductility. For example, the annealed and ST samples showed an El of 27.5% and 37.5%, respectively. The STA1 sample exhibited an El of 35%. Note that the STA2 sample exhibited lower strength and ductility compared to the other samples owing to the coarse precipitates.

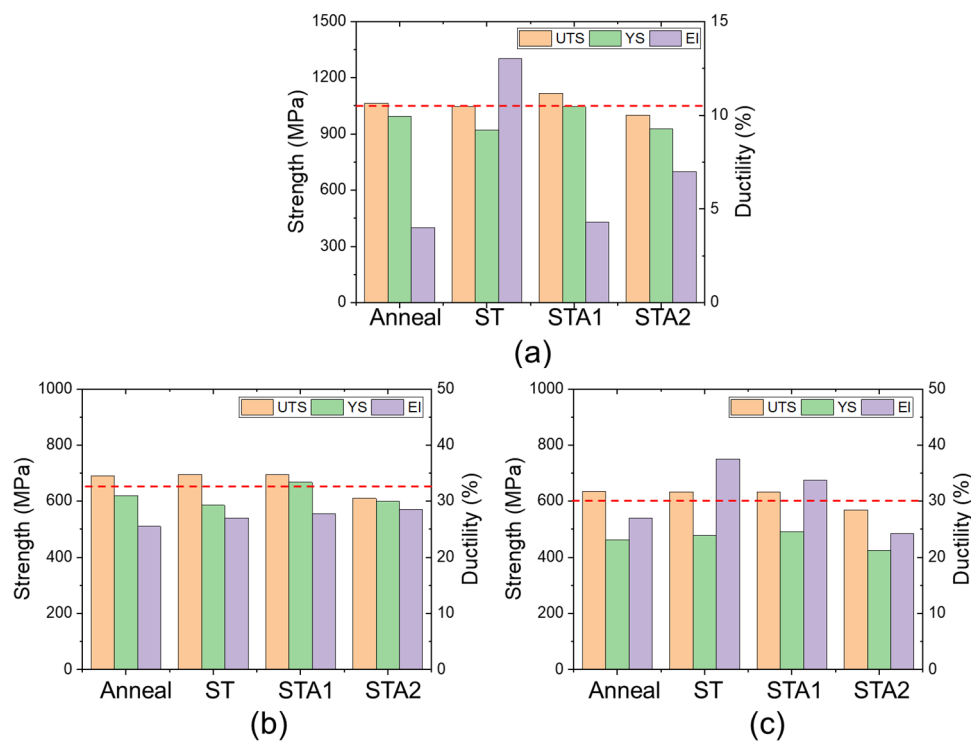


Figure 5. Tensile properties of the heat-treated samples tested at (a) room temperature, (b) 600 °C, and (c) 650 °C.

The UTS and EI of the laser melting deposited TC31 samples after post-heat treatments tested at room temperature and 650 °C are shown in Table 2, as compared to TC31 manufactured by conventional methods [26]. The laser melting deposited TC31 samples after properly selected heat treatments exhibited a better combination between strength and ductility both at room temperature and 650 °C. For example, the ST sample exhibited a strength of 1047 MPa and ductility of 13.0% at room temperature, while the conventional ST sample exhibited a similar strength but much lower ductility, 8.0%. The ST sample and STA1 sample also exhibited both higher strength and ductility than that of the conventional TC31 samples after similar heat treatments.

Table 2. Mechanical properties of TC31 fabricated by LMD and conventional technique at room temperature and 650 °C.

Heat Treatments	Room Temperature			650 °C			Ref.
	UTS/MPa	YS/MPa	EI%	UTS/MPa	YS/MPa	EI%	
Annealed: 800 °C/2 h	1064	993	4.0	635	462	27.0	This study
ST: 980 °C/2 h	1047	920	13.0	634	477	30.0	
ST: 980 °C/2 h Aging: 650 °C/2 h	1117	1045	4.3	633	492	34.0	
ST: 980 °C/2 h Aging: 750 °C/2 h	1001	928	7.0	570	426	24.0	
ST: 980 °C/2 h	1050	900	8.0	605	400	20.0	
ST: 980 °C/2 h Aging: 600 °C/2 h	1080	900	8.0	575	370	30.0	[29]
ST: 980 °C/2 h Aging: 750 °C/2 h	1000	900	2.5	545	350	22.0	

3.3. Fracture Surface Analysis

Fracture surface analysis of the samples was performed to understand the tensile properties. The fractography of the samples tested at room temperature and high temperature are shown in Figures 6 and 7, respectively.

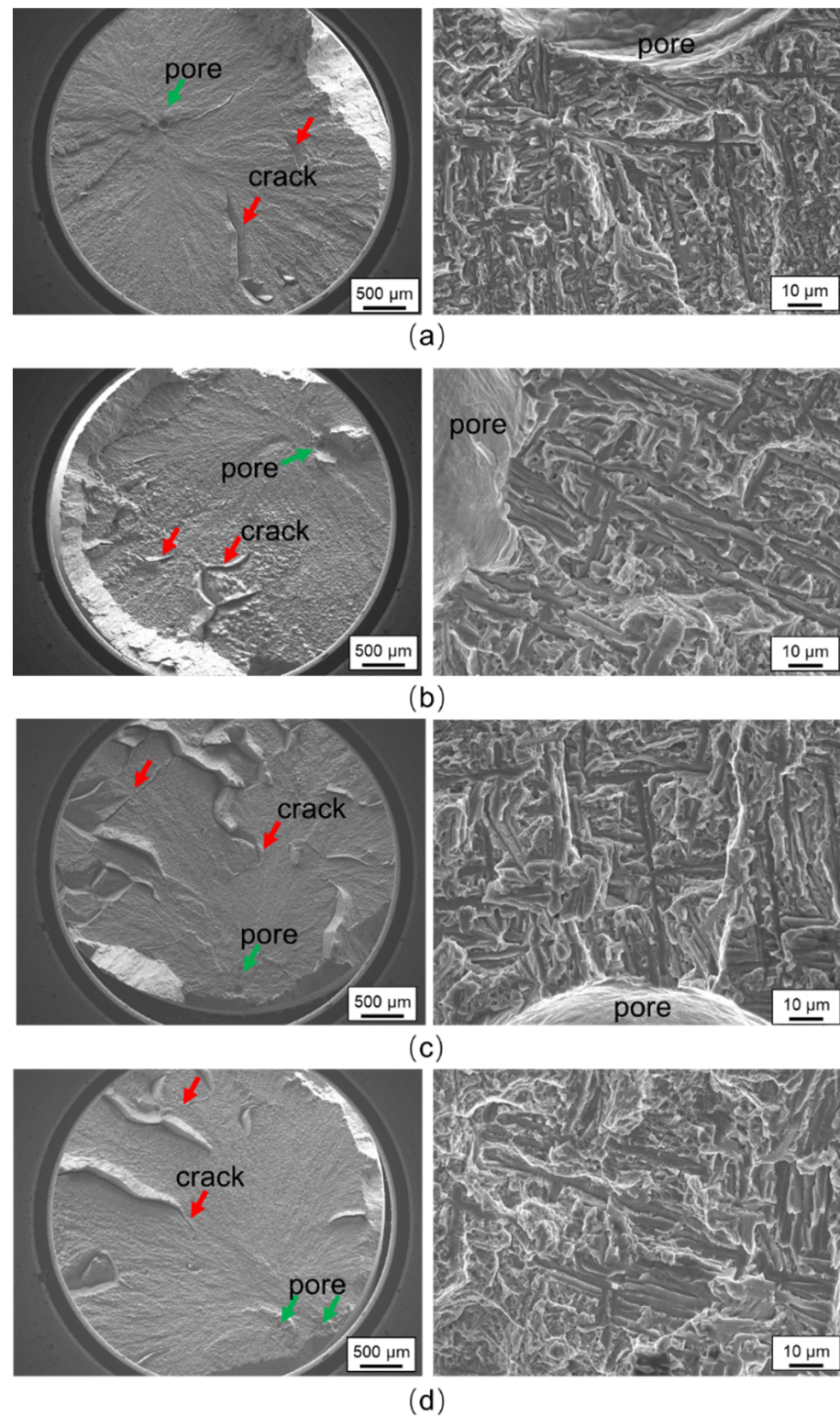


Figure 6. Fracture surfaces of the samples tested at room temperature: (a) annealed, (b) ST, (c) STA1, and (d) STA2.

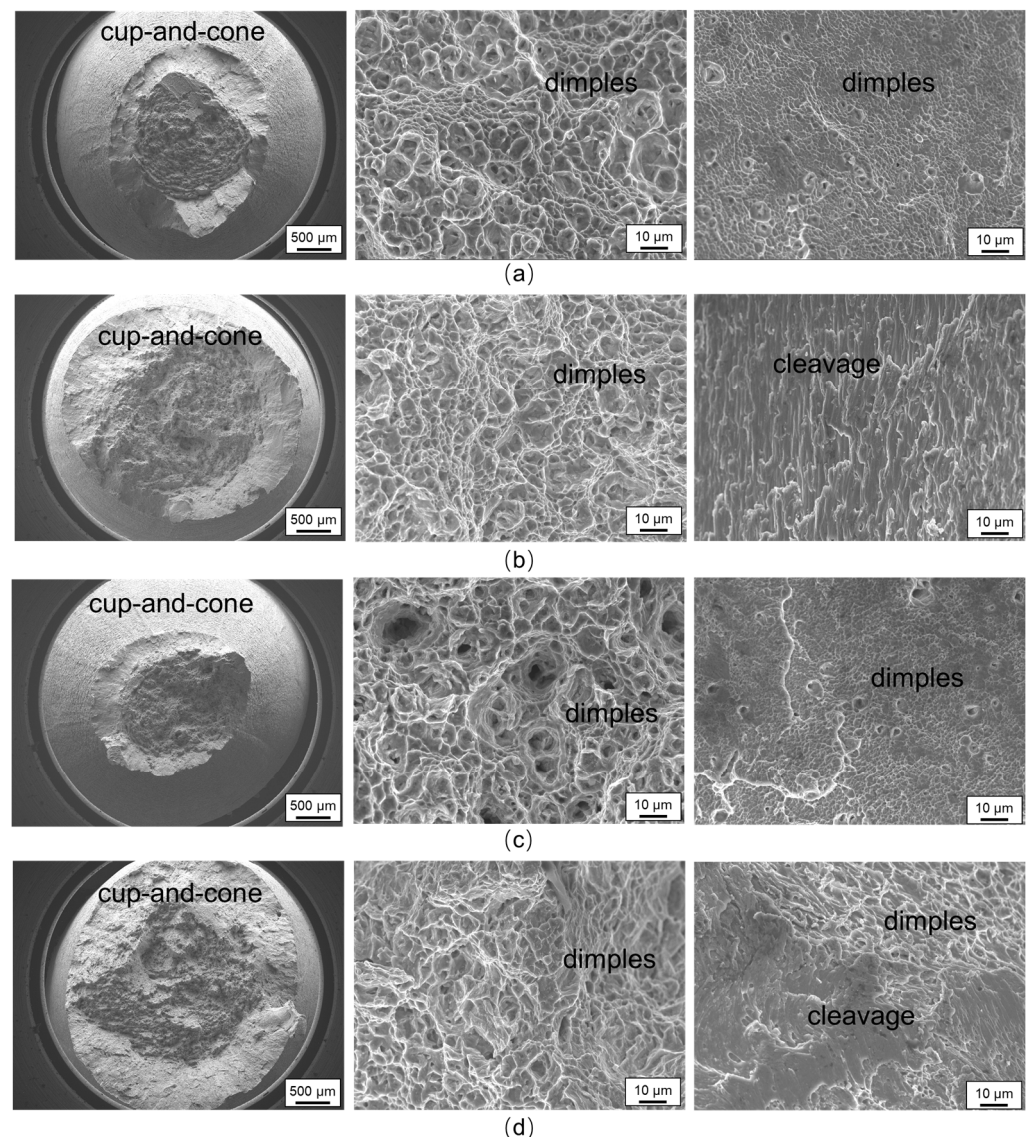


Figure 7. Fracture surfaces of the samples: (a) STA1, (b) STA2 tested at 600 °C, and (c) STA1, (d) STA2 at 650 °C.

When tested at room temperature, the samples exhibited brittle fractures, as shown in Figure 6. The cracks tended to nucleate at pores and then propagate along the prior β grain boundaries. Cracks were also formed along the prior β boundaries as indicated by arrows. In addition, high magnification images also indicated that the microcracks formed along the boundaries of the lamellar grains. Therefore, these samples exhibited relatively low ductility at room temperature.

When tested at 600 and 650 °C, the samples exhibited cup-and-cone shapes, and fibrous surfaces, indicating typical ductile fractures, as shown in Figure 7. However, high-magnification images revealed very fine dimples in the samples. In addition, there were some cleavages observed in the STA2 samples tested at 600 and 650 °C.

4. Conclusions

Highly dense LMD-built TC31 alloy samples with a desirable combination of tensile strength and ductility at room temperature and high temperature were successfully fabricated via post-heat treatments in this work. The following conclusions can be drawn.

(1) The LMD-built sample exhibited columnar structures with very fine α -laths inside. Annealing at 800 °C resulted in a fine $\alpha + \beta$ lamellar structure consisting of thin α -laths

and β -films; both of their thicknesses are less than 1 μm . Solution treatment at 980 $^{\circ}\text{C}$ created a coarse $\alpha + \beta$ lamellar structure, of which the thickness is approximately 2–3 μm . Subsequent aging at 650 and 750 $^{\circ}\text{C}$ did not significantly change the coarse lamellar structure. However, aging at 650 $^{\circ}\text{C}$ led to the formation of nanoscale α precipitates within the remaining β , and aging at 750 $^{\circ}\text{C}$ resulted in coarse α precipitates within the remaining β .

(2) At room temperature, the solution-treated samples exhibited the best combination of strength and ductility, UTS of 1047 MPa and El of 13.0%, which is superior to the wrought TC31 counterparts, UTS of 1050 MPa, and El of 8.0%. At 600 $^{\circ}\text{C}$, the annealed, solution-treated samples exhibited similar strength and ductility, UTS of \sim 650 MPa and El of \sim 25%. At 650 $^{\circ}\text{C}$, the solution-treated samples and the samples aged at 650 $^{\circ}\text{C}$ exhibited better combinations of strength and ductility, UTS of 630 MPa and El of 30%, which are much superior to those of the wrought TC31 counterparts. Aging at 750 $^{\circ}\text{C}$ resulted in low strength and ductility both at room temperature and high temperature because of coarse α precipitates.

(3) The sample after solution treatment at 980 $^{\circ}\text{C}$ and subsequent aging at 650 $^{\circ}\text{C}$ obtained an attractive combination of strength and ductility due to the synergistic effect of the soft $\alpha + \beta$ lamellar structure and hard fine α precipitates.

Author Contributions: Conceptualization, H.L. and B.G.; methodology, Y.Z.; formal analysis, H.L.; investigation, H.L.; resources, B.G.; data curation, D.S.; writing—original draft preparation, H.L.; writing—review and editing, Y.Z.; supervision, B.G. All authors have read and agreed to the published version of the manuscript.

Funding: This research received no external funding.

Data Availability Statement: Not applicable.

Conflicts of Interest: The authors declare no conflict of interest.

References

1. Xiong, Z.; Pang, X.; Liu, S.; Li, Z.; Misra, R.D.K. Hierarchical refinement of nickel-microalloyed titanium during additive manufacturing. *Scr. Mater.* **2021**, *195*, 113727. [[CrossRef](#)]
2. Yue, H.-Y.; Peng, H.; Su, Y.-J.; Wang, X.-P.; Chen, Y.-Y. Microstructure and high-temperature tensile property of TiAl alloy produced by selective electron beam melting. *Rare Met.* **2021**, *40*, 3635–3644. [[CrossRef](#)]
3. DebRoy, T.; Wei, H.L.; Zuback, J.S.; Mukherjee, T.; Elmer, J.W.; Milewski, J.O.; Beese, A.M.; Wilson-Heid, A.; De, A.; Zhang, W. Additive manufacturing of metallic components—Process, structure and properties. *Prog. Mater. Sci.* **2018**, *92*, 112–224. [[CrossRef](#)]
4. Liang, C.-Y.; Jiang, X.-J.; Ji, R.-L.; Li, B.-E.; Zou, X.-R.; Wang, H.-S.; Hao, J.-Z.; Yang, T. Preparation and surface modification of 3D printed Ti–6Al–4V porous implant. *Rare Met.* **2021**, *40*, 1164–1172. [[CrossRef](#)]
5. Wang, M.; Li, H.-Q.; Guo, H.; Feng, L.; Liu, S.-Y.; Fang, X.-Y. Evolution of microstructure and intervariant boundaries of α phase in electron beam melted and heat-treated Ti–6Al–4V alloy. *Rare Met.* **2021**, *40*, 2118–2126. [[CrossRef](#)]
6. Herzog, D.; Seyda, V.; Wycisk, E.; Emmelmann, C. Additive manufacturing of metals. *Acta Mater.* **2016**, *117*, 371–392. [[CrossRef](#)]
7. Shamsaei, N.; Yadollahi, A.; Bian, L.; Thompson, S.M. An overview of Direct Laser Deposition for additive manufacturing; Part II: Mechanical behavior, process parameter optimization and control. *Add. Manuf.* **2015**, *8*, 12–35. [[CrossRef](#)]
8. Thompson, S.M.; Bian, L.; Shamsaei, N.; Yadollahi, A. An overview of Direct Laser Deposition for additive manufacturing; Part I: Transport phenomena, modeling and diagnostics. *Add. Manuf.* **2015**, *8*, 36–62. [[CrossRef](#)]
9. Azarniya, A.; Colera, X.G.; Mirzaali, M.J.; Sovizi, S.; Bartolomeu, F.; St Węglowski, M.K.; Wits, W.W.; Yap, C.Y.; Ahn, J.; Miranda, G.; et al. Additive manufacturing of Ti–6Al–4V parts through laser metal deposition (LMD): Process, microstructure, and mechanical properties. *J. Alloys Compd.* **2019**, *804*, 163–191. [[CrossRef](#)]
10. Frazier, W.E. Metal Additive Manufacturing: A Review. *J. Mater. Eng. Perform.* **2014**, *23*, 1917–1928. [[CrossRef](#)]
11. Narayana, P.L.; Lee, S.; Choi, S.-W.; Li, C.-L.; Park, C.H.; Yeom, J.-T.; Reddy, N.S.; Hong, J.-K. Microstructural response of β -stabilized Ti–6Al–4V manufactured by direct energy deposition. *J. Alloys Compd.* **2019**, *811*, 152021. [[CrossRef](#)]
12. Li, R.; Wang, H.; He, B.; Li, Z.; Zhu, Y.; Zheng, D.; Tian, X.; Zhang, S. Effect of α texture on the anisotropy of yield strength in Ti–6Al–2Zr–1Mo–1V alloy fabricated by laser directed energy deposition technique. *Mater. Sci. Eng. A* **2021**, *824*, 141771. [[CrossRef](#)]
13. Simonelli, M.; Tse, Y.Y.; Tuck, C. Effect of the build orientation on the mechanical properties and fracture modes of SLM Ti–6Al–4V. *Mater. Sci. Eng. A* **2014**, *616*, 1–11. [[CrossRef](#)]
14. Keist, J.S.; Palmer, T.A. Role of geometry on properties of additively manufactured Ti-6Al-4V structures fabricated using laser based directed energy deposition. *Mater. Des.* **2016**, *106*, 482–494. [[CrossRef](#)]

15. Zhu, Y.; Tian, X.; Li, J.; Wang, H. The anisotropy of laser melting deposition additive manufacturing Ti–6.5Al–3.5Mo–1.5Zr–0.3Si titanium alloy. *Mater. Des.* **2015**, *67*, 538–542. [[CrossRef](#)]
16. Carroll, B.E.; Palmer, T.A.; Beese, A.M. Anisotropic tensile behavior of Ti-6Al-4V components fabricated with directed energy deposition additive manufacturing. *Acta Mater.* **2015**, *87*, 309–320. [[CrossRef](#)]
17. Nourollahi, A.; Shoja Razavi, R.; Barekat, M. Microstructural investigation of direct laser deposition of the Ti–6Al–4V alloy by different melt pool protection conditions. *J. Mater. Res. Technol.* **2021**, *13*, 590–601. [[CrossRef](#)]
18. Wolff, S.; Lee, T.; Faierson, E.; Ehmann, K.; Cao, J. Anisotropic properties of directed energy deposition (DED)-processed Ti–6Al–4V. *J. Manuf. Process.* **2016**, *24*, 397–405. [[CrossRef](#)]
19. Zhu, Y.; Liu, D.; Tian, X.; Tang, H.; Wang, H. Characterization of microstructure and mechanical properties of laser melting deposited Ti–6.5Al–3.5Mo–1.5Zr–0.3Si titanium alloy. *Mater. Des.* **2014**, *56*, 445–453. [[CrossRef](#)]
20. Ren, Y.M.; Lin, X.; Fu, X.; Tan, H.; Chen, J.; Huang, W.D. Microstructure and deformation behavior of Ti-6Al-4V alloy by high-power laser solid forming. *Acta Mater.* **2017**, *132*, 82–95. [[CrossRef](#)]
21. Wolff, S.J.; Lin, S.; Faierson, E.J.; Liu, W.K.; Wagner, G.J.; Cao, J. A framework to link localized cooling and properties of directed energy deposition (DED)-processed Ti-6Al-4V. *Acta Mater.* **2017**, *132*, 106–117. [[CrossRef](#)]
22. Zhao, Z.; Chen, J.; Tan, H.; Zhang, G.; Lin, X.; Huang, W. Achieving superior ductility for laser solid formed extra low interstitial Ti-6Al-4V titanium alloy through equiaxial alpha microstructure. *Scr. Mater.* **2018**, *146*, 187–191. [[CrossRef](#)]
23. Wang, C.-S.; Li, C.-L.; Zuo, Y.-T.; Hong, J.-K.; Choi, S.-W.; Zhang, G.-D.; Mei, Q.; Park, C.H.; Yeom, J.-T. Tailoring bimodal structure for high strength and ductility in pure titanium manufactured via laser powder bed fusion. *J. Alloys Compd.* **2022**, *901*, 163590. [[CrossRef](#)]
24. Li, C.-L.; Hong, J.-K.; Narayana, P.L.; Choi, S.-W.; Lee, S.W.; Park, C.H.; Yeom, J.-T.; Mei, Q. Realizing superior ductility of selective laser melted Ti-6Al-4V through a multi-step heat treatment. *Mater. Sci. Eng. A* **2021**, *799*, 140367. [[CrossRef](#)]
25. Cai, C.; Wu, X.; Liu, W.; Zhu, W.; Chen, H.; Qiu, J.C.D.; Sun, C.N.; Liu, J.; Wei, Q.; Shi, Y. Selective laser melting of near- α titanium alloy Ti-6Al-2Zr-1Mo-1V: Parameter optimization, heat treatment and mechanical performance. *J. Mater. Sci. Technol.* **2020**, *57*, 51–64. [[CrossRef](#)]
26. Zhang, W.-J.; Song, X.-Y.; Hui, S.-X.; Ye, W.-J.; Wang, W.-Q. Phase precipitation behavior and tensile property of a Ti–Al–Sn–Zr–Mo–Nb–W–Si titanium alloy. *Rare Met.* **2018**, *37*, 1064–1069. [[CrossRef](#)]
27. Wang, Z.; Sun, L.; Ke, W.; Zeng, Z.; Yao, W.; Wang, C. Laser Oscillating Welding of TC31 High-Temperature Titanium Alloy. *Metals* **2020**, *10*, 1185. [[CrossRef](#)]
28. Dang, K.; Wang, K.; Liu, G. Dynamic Softening and Hardening Behavior and the Micro-Mechanism of a TC31 High Temperature Titanium Alloy Sheet within Hot Deformation. *Materials* **2021**, *14*, 6515. [[CrossRef](#)] [[PubMed](#)]
29. Zhang, W.J.; Song, X.Y.; Hui, S.X.; Ye, W.J.; Wang, Y.L.; Wang, W.Q. Tensile behavior at 700 °C in Ti–Al–Sn–Zr–Mo–Nb–W–Si alloy with a bi-modal microstructure. *Mater. Sci. Eng. A* **2014**, *595*, 159–164. [[CrossRef](#)]